

**An efficient estimation of time-varying parameters of dynamic models by combining offline batch optimization and online data assimilation**

Yohei Sawada<sup>1</sup>,

<sup>1</sup> Institute of Engineering Innovation, the University of Tokyo, Tokyo, Japan

Corresponding author: Y. Sawada, Institute of Engineering Innovation, the University of Tokyo, Tokyo, Japan, 2-11-6, Yayoi, Bunkyo-ku, Tokyo, Japan, yohei.sawada@sogo.t.u-tokyo.ac.jp

## **Abstract**

It is crucially important to estimate unknown parameters in earth system models by integrating observation and numerical simulation. For many applications in earth system sciences, the optimization method which allows parameters to temporally change is required. Here I present an efficient and practical method to estimate the time-varying parameters of relatively low dimensional models. I propose combining offline batch optimization and online data assimilation. In the newly proposed method, called Hybrid Offline Online Parameter Estimation with Particle Filtering (HOOPE-PF), I constrain the estimated model parameters in sequential data assimilation to the result of offline batch optimization in which the posterior distribution of model parameters is obtained by comparing the simulated and observed climatology. The HOOPE-PF outperforms the original sampling-importance-resampling particle filter in the synthetic experiment with the toy model and the real-data experiment with the conceptual hydrological model. The advantage of HOOPE-PF is that the performance of the online data assimilation is not greatly affected by the hyperparameter of ensemble data assimilation which contributes to inflating the ensemble variance of estimated parameters.

## **Plain Language Summary**

In Earth system sciences, numerical models are crucially important tools to understand, monitor, and predict earth systems. Most of numerical models in earth system sciences have the unknown coefficients of equations, which are called model parameters. Since it is impossible to directly measure model parameters, many previous works have developed methods to infer these model parameters by comparing the result of simulation and observation data. These methods can be classified into two categories: online data assimilation and offline batch optimization. In the online data assimilation, the model parameters are sequentially updated by frequently integrating each observation into simulation while the long-term differences between simulation and observation are minimized in the offline batch optimization. Here I present the efficient and practical parameter optimization method by combining these two strategies. The proposed method is found to be appropriate to estimate the time-varying model parameters without the intensive calibration of hyperparameters of online data assimilation.

## **Key Points**

An efficient and practical method to estimate time-varying model parameters is proposed.

Particle filtering can be stabilized by combining offline batch optimization and online data assimilation.

The new method is successfully applied to the Lorenz 63 model and the conceptual hydrological model.

## 1. Introduction

In Earth system sciences, numerical models are crucially important tools to understand, monitor, and predict earth systems. Most of numerical models in earth system sciences have many unknown parameters which cannot be directly determined by current theory and cannot be directly measured. This uncertainty in model parameters substantially affects the skill of numerical models to simulate the real phenomena. It is a grand challenge to infer the model parameters by integrating observations and models. Although model parameters are often assumed to be time-invariant, there are time-varying parameters in the practical applications due to incomplete parameterizations and unconsidered dynamics that control parameters (e.g., Reichert et al. 2021). It is beneficial to develop the efficient and practical parameter estimation method which allows parameters to temporally change.

To estimate the time-varying parameters, online parameter estimation by sequential data assimilation has been recognized as the useful method. Since ensemble data assimilation such as Ensemble Kalman filter (EnKF) and Particle Filter (PF) can sequentially adjust model parameters using real-time observations, it can be easily applied to the estimation of the time-varying parameters. Ruiz et al. (2013a) applied the Local Ensemble Transform Kalman Filter (LETKF; Hunt et al. 2007) to jointly estimate state variables and parameters in a simple low-resolution General Circulation Model (GCM). They successfully estimated the time-varying parameters by sequentially adjusting them in the idealized experiment. Pathiraja et al. (2018) successfully detected the land use change in a river basin by applying the locally linear dual EnKF proposed by Pathiraja et al. (2016) to estimate temporal changes in the parameters of hydrological models. Sawada and Hanazaki (2020) applied PF to a socio-hydrological model proposed by Di Baldassarre et al. (2013), in which flood-human interactions are simulated. They successfully estimated the time-varying parameters driven by unknown social dynamics in the idealized experiment.

Whenever parameters are adjusted by ensemble data assimilation, the estimated ensemble variance of updated parameters is always smaller than that of the background. If the ensemble variance is too small compared to the observation error variances, the information of observation cannot impact the state and parameter estimation. To avoid this filter degeneracy (Anderson 2007), it is crucially important to maintain the appropriate ensemble variance of updated parameters. Many parameter evolution models

(they are often called covariance inflation methods in the meteorological literature) have been proposed to maintain the ensemble variance of estimated parameters. Moradkhani et al. (2005a) simply added the Gaussian noise, whose variance is proportional to the ensemble variance of the background, to parameters of each ensemble member after adjusting them by the sampling-importance-resampling PF. Moradkhani et al. (2005b) used the kernel smoother with location shrinkage (Liu and West 2001) to perturb the updated parameters and maintain the ensemble variance of parameters in their dual EnKF. Similar strategies to Moradkhani et al. (2005a, 2005b) have been used in many previous works (e.g., Yan and Moradkhani 2016; Pathiraja et al. 2016; Ait-El-Fquih and Hoteit 2017; Pathiraja et al. 2018; Sawada and Hanazaki 2020). It has been shown effective to evaluate the perturbed parameters by running a numerical model again and iteratively sampling the new perturbed parameters (e.g., Moradkhani et al. 2012; Vrugt et al. 2013; Abbaszadeh et al. 2018), although the computational cost is increased by this strategy. Ruiz et al. (2013) discussed how to objectively determine the appropriate variance of updated parameters using the ensemble variance of the background and updated state variables. Kotsuki et al. (2018) used the relaxation to prior spread method (Whitaker and Hamil 2012) to constrain the ensemble variance of parameters to the initial prescribed variance in their LETKF framework.

As an alternative approach of the parameter estimation, offline batch optimization, in which model parameters are optimized based on the statistics of the long-term difference between simulation and observation, remains highly popular. The advantage of the offline batch optimization is that non-parametric Bayesian inference can easily be applied in this framework, so that the reliable uncertainty estimation of model parameters can be obtained. Since it is necessary to iteratively perform the long-term integration of a numerical model with different parameters, the direct application of the offline batch optimization to the models in earth system sciences is computationally expensive (e.g., Laloy and Vrugt 2012). However, the computational cost of the offline batch optimization can be dramatically reduced by replacing the responses of numerical models to parameters with machine learning models called surrogate models. For example, Sawada (2020) used the Gaussian process regression (Rasmussen and Williams 2006) to mimic the relationship between parameters in a land surface model and simulated microwave brightness temperature which are sensitive to soil moisture and vegetation water content. By evaluating parameters based on the computationally cheap statistical surrogate model, the Markov Chain Monte Carlo (MCMC) sampler could be efficiently applied to optimize soil and vegetation parameters of the land surface model. Zhang et al. (2020) developed

the adaptive approach to construct the surrogate model and applied it to the parameter inference of a groundwater model. Parente et al. (2019) applied the active subspace method (Constantine et al. 2014) to efficiently construct a surrogate model and calibrate parameters of a hydrological model. Dunbar et al. (2021) successfully performed the surrogate model based MCMC and realized the uncertainty quantification of convective parameters in an idealized GCM with only  $O(10^2)$  model runs.

Several studies proposed combining data assimilation and offline batch optimization with machine learning (e.g., Cleary et al. 2021; Lunderman et al. 2021; Tomizawa and Sawada 2021). Despite the high potential of the synergetic effect of the online data assimilation and the offline batch optimization, to my best knowledge, there is no contribution to the estimation of time-varying parameters by combining them. The aim of this study is to develop an efficient and practical model parameter optimization method which can allow parameters to temporally vary by combining online PF and offline batch optimization with the surrogate model based MCMC. First, I obtained the posterior distribution of parameters by the offline batch optimization based on the climatology of simulation and observation. Second, I performed online PF in which the estimated parameters are constrained to the posterior distribution calculated by the offline batch optimization. I found that the sensitivity of the PF's performance to a hyperparameter in a parameter evolution model is minimal in the proposed method. Therefore, the proposed method contributes to solving the issues in the maintenance of ensemble variance discussed above. I will demonstrate this feature in the idealized experiment with the Lorenz 63 model (Lorenz 1963) and the real-data experiment with the HYMOD lumped hydrological model (Moore 2007).

## 2. Method

### 2.1. Online data assimilation: Particle Filtering

In this study, I used the Sampling-Importance-Resampling Particle Filter (SIRPF) algorithm as a method of data assimilation. The implementation of Moradkhani et al. (2005a) was mostly used in this study. A discrete state-space dynamics system is defined as follows:

$$\mathbf{x}(t) = f(\mathbf{x}(t-1), \boldsymbol{\theta}(t-1), \mathbf{u}(t-1)) + \mathbf{q}(t-1) \quad (1)$$

where  $\mathbf{x}(t)$  is the state variable,  $\boldsymbol{\theta}(t)$  is the model parameters,  $\mathbf{u}(t)$  is the external forcing, and  $\mathbf{q}(t)$  is the noise process which represents the model error at time  $t$ .  $f(\cdot)$  is the dynamic model. Note that the model parameters are the function of  $t$ , so that I assumed

that I have time-varying parameters. Data assimilation needs to formulate an observation process:

$$\mathbf{y}^f(t) = h(\mathbf{x}(t)) + \mathbf{r}(t) \quad (2)$$

where  $\mathbf{y}^f(t)$  is the simulated observation at time  $t$ ,  $\mathbf{r}(t)$  is the noise process which represents observation error at time  $t$ .  $h(\cdot)$  is the observation operator. The purpose of PF (and any other sequential data assimilation methods) is to obtain the posterior distribution of the state variables and parameters based on the Bayesian update:

$$p(\mathbf{x}(t), \boldsymbol{\theta}(t) | \mathbf{y}^o(1:t)) \propto p(\mathbf{y}^o(t) | \mathbf{x}(t), \boldsymbol{\theta}(t)) p(\mathbf{x}(t), \boldsymbol{\theta}(t) | \mathbf{y}^o(1:t-1)) \quad (3)$$

where  $p(\mathbf{x}(t), \boldsymbol{\theta}(t) | \mathbf{y}^o(1:t))$  is the posterior probability of the state variables  $\mathbf{x}(t)$  and parameters  $\boldsymbol{\theta}(t)$  given all observation up to time  $t$ ,  $\mathbf{y}^o(1:t)$ . The prior knowledge,  $p(\mathbf{x}(t), \boldsymbol{\theta}(t) | \mathbf{y}^o(1:t-1))$ , is updated using the likelihood,  $p(\mathbf{y}^o(t) | \mathbf{x}(t), \boldsymbol{\theta}(t))$  which includes the information of the new observation at time  $t$ . PF directly approximates equation (3) by Monte Carlo simulation.

The implementation of SIRPF in this study is as follows:

1. Forecasting the model state variables and parameters from time  $t-1$  to  $t$  using the ensemble simulation.

$$\mathbf{x}_i^f(t) = f(\mathbf{x}_i^a(t-1), \boldsymbol{\theta}_i^a(t-1), \mathbf{u}(t-1)) \quad (4)$$

$$\boldsymbol{\theta}_i^f(t) = \boldsymbol{\theta}_i^a(t-1) \quad (5)$$

where superscripts  $f$  and  $a$  show forecasted and updated variables, respectively. Subscript  $i$  shows the ensemble number. Equation (5) implies that no dynamics is assumed for the model parameters in the forecast step.

2. Calculating the simulated observations for all ensembles:

$$\mathbf{y}_i^f(t) = h(\mathbf{x}_i^f(t)) \quad (6)$$

3. Calculating the weights for all ensembles:

$$w_i = \frac{L(\mathbf{y}^o(t), \mathbf{x}_i^f(t), \boldsymbol{\theta}_i^f(t))}{\sum_{k=1}^N L(\mathbf{y}^o(t), \mathbf{x}_k^f(t), \boldsymbol{\theta}_k^f(t))} \quad (7)$$

where  $w_i$  is the normalized weight for the  $i$ th ensemble member, and  $N$  is the ensemble size.  $L$  is the likelihood function. In this study, I assumed that the observation error follows the Gaussian distribution, so that  $L$  can be formulated as follows:

$$L = \frac{1}{\sqrt{\det(2\pi\mathbf{R})}} \exp\left(-\frac{1}{2}(\mathbf{y}^o(t) - \mathbf{y}_i^f(t))^T \mathbf{R}^{-1}(\mathbf{y}^o(t) - \mathbf{y}_i^f(t))\right) \quad (8)$$

where  $\mathbf{R}$  is the covariance matrix of the observation error.

4. Resampling ensemble members based on the normalized weights. The normalized weights  $w_i$  is recognized as the probability that the ensemble  $i$  is selected after

resampling. The resampled state variables and parameters are defined as  $\mathbf{x}_i^{resamp}$  and  $\boldsymbol{\theta}_i^{resamp}$ , respectively.

5. Adding the perturbation to the state variables and parameters to maintain the appropriate ensemble variances:

$$\mathbf{x}_i^a = \mathbf{x}_i^{resamp} + \boldsymbol{\varepsilon}_{i,state} \quad (9)$$

$$\boldsymbol{\varepsilon}_{i,state} \sim N(0, S_{state} \times Var^x) \quad (10)$$

$$\boldsymbol{\theta}_i^a = \boldsymbol{\theta}_i^{resamp} + \boldsymbol{\varepsilon}_{i,para} \quad (11)$$

$$\boldsymbol{\varepsilon}_{i,para} \sim N(0, S_{para} \times Var^\theta) \quad (12)$$

where  $N(\cdot)$  is the Gaussian distribution,  $Var^x$  and  $Var^\theta$  are the ensemble variances of the state variables  $\mathbf{x}_i^f(t)$  and parameters  $\boldsymbol{\theta}_i^f(t)$  in the background field, respectively.

$S_{state}$  and  $S_{para}$  are the ‘‘inflation’’ hyperparameters. The performance of the original PF is sensitive to them. Several approaches to determine them objectively and adaptively have been proposed (e.g., Leisenring and Moradkhani 2012; Sawada and Hanazaki 2020). In this study, I did not apply these adaptive approaches and fixed these parameters. I will show that the performance of PF is not sensitive to these hyperparameters in the proposed method.

## 2.2. Offline batch optimization

In the offline batch optimization of this paper, the parameters are assumed to be time-invariant. A discrete state-space dynamics system is re-written as:

$$\mathbf{x}(t) = f(\mathbf{x}(t-1), \hat{\boldsymbol{\theta}}, \mathbf{u}(t-1)) + \mathbf{q}(t-1) \quad (13)$$

$$\mathbf{y}^f(t) = h(\mathbf{x}(t)) + \mathbf{r}(t) \quad (14)$$

where  $\hat{\boldsymbol{\theta}}$  is the time-invariant model parameter. In this study, some climatological indices were calculated based on the long-term averages of the timeseries of the simulated observation  $\mathbf{y}^f(t)$  and the real observation  $\mathbf{y}^o(t)$ . Since these climatological indices are designed to be independent to the initial condition, the problem of the offline batch optimization can be simplified as:

$$\boldsymbol{\gamma}^f = g(\hat{\boldsymbol{\theta}}) \quad (15)$$

where  $\boldsymbol{\gamma}^f$  is the simulated climatological index.  $g(\cdot)$  is the forward map. The purpose of the offline batch optimization in this study is to obtain the posterior probabilistic distribution of  $\hat{\boldsymbol{\theta}}$  based on the simulated climatological index  $\boldsymbol{\gamma}^f$  and the observed climatological index  $\boldsymbol{\gamma}^o$ .



It is generally difficult to perform the Bayesian inference using equation (15) since  $g(\cdot)$  is computationally expensive. In this study, the surrogate model of  $g(\cdot)$  was developed by the Gaussian process regression (Rasmussen and Williams 2006). First, I generated 500 ensemble members of model parameters by the pseudo-Monte Carlo sampling. Second, I performed the numerical simulation with the 500 parameter ensembles in parallel. Third, I constructed the statistical surrogate model from the data of the 500  $\hat{\boldsymbol{\theta}}-\boldsymbol{\gamma}^f$  combinations by the Gaussian process regression. The surrogate model replaces equation (15) with:

$$\boldsymbol{\gamma}^f = g^{(s)}(\hat{\boldsymbol{\theta}}) \quad (16)$$

where  $g^{(s)}(\cdot)$  is the computationally cheap surrogate model of  $g(\cdot)$ .

The posterior of  $\hat{\boldsymbol{\theta}}$  was obtained by the MCMC sampler. I used the Metropolis-Hastings algorithm (Hastings 1970). The implementation of the MCMC sampler is the following:

1. For each iteration  $i$ , generate a candidate parameter vector  $\hat{\boldsymbol{\theta}}_c$ . This candidate is sampled from the proposal distribution  $q(\hat{\boldsymbol{\theta}}_c|\hat{\boldsymbol{\theta}}_i)$ .

2. Calculating the acceptance probability of  $\hat{\boldsymbol{\theta}}_c$ ,  $\alpha(\hat{\boldsymbol{\theta}}_i, \hat{\boldsymbol{\theta}}_c)$  by the following equations (Cleary et al. 2021):

$$\alpha(\hat{\boldsymbol{\theta}}_i, \hat{\boldsymbol{\theta}}_c) = \exp\left(\Phi^{(s)}(\hat{\boldsymbol{\theta}}_i) - \Phi^{(s)}(\hat{\boldsymbol{\theta}}_c)\right) \quad (17)$$

$$\Phi^{(s)}(\hat{\boldsymbol{\theta}}) = \frac{1}{2} \|\boldsymbol{\gamma}^o - g^{(s)}(\hat{\boldsymbol{\theta}})\|_{R_{gp}(\hat{\boldsymbol{\theta}})+R_o}^2 \quad (18)$$

where  $R_{gp}(\hat{\boldsymbol{\theta}})$  and  $R_o$  are the error variances of  $g^{(s)}(\hat{\boldsymbol{\theta}})$  and observation, respectively. The acceptance probability is calculated based on the square difference between the simulated and observed climatological indices normalized by the total error variance of the Gaussian process and the observation measurement.

3. Determine if  $\hat{\boldsymbol{\theta}}_c$  is accepted as a new parameter or not. A random number,  $b$ , is generated from the uniform distribution of [0,1]. Then,

If  $b \leq \alpha(\hat{\boldsymbol{\theta}}_i, \hat{\boldsymbol{\theta}}_c)$ , accept the candidate parameter and  $\hat{\boldsymbol{\theta}}_{i+1} = \hat{\boldsymbol{\theta}}_c$

If  $b > \alpha(\hat{\boldsymbol{\theta}}_i, \hat{\boldsymbol{\theta}}_c)$ , reject the candidate parameter and  $\hat{\boldsymbol{\theta}}_{i+1} = \hat{\boldsymbol{\theta}}_i$

I repeated this iteration 500,000 times in this study and discarded the first 100,000 iterations as the spin-up period. In this study,  $q(\hat{\boldsymbol{\theta}}_c|\hat{\boldsymbol{\theta}}_i)$  is assumed to be Gaussian with zero mean. Since the Gaussian process can provide both mean and variance of their estimation in each point, it is straightforward to obtain  $R_{gp}(\hat{\boldsymbol{\theta}})$  whenever  $g^{(s)}(\hat{\boldsymbol{\theta}})$  is evaluated. To calculate  $R_o$ , I randomly chose the subset of the observation's timeseries and generate 1,000 observed climatological index  $\boldsymbol{\gamma}^o$ . The variance of the observed climatological index was calculated as the variance of these 1,000  $\boldsymbol{\gamma}^o$ . In addition, I

randomly chose  $\boldsymbol{y}^o$  from these subsets of the observed climatological index in every 100 iterations of MCMC. This procedure was found to be necessary to obtain the posterior of the time-invariant  $\hat{\boldsymbol{\theta}}$  which can explain the non-stationary observation climatology.

### 2.3. Hybrid Offline Online Parameter Estimation with Particle Filtering (HOOPE-PF)

The schematic of the proposed method, Hybrid Offline Online Parameter Estimation with Particle Filtering (HOOPE-PF), is shown in Figure 1. The fundamental idea is that the posterior of PF,  $p(\boldsymbol{x}(t), \boldsymbol{\theta}(t) | \boldsymbol{y}^o(1:t))$  (see section 2.1), is constrained by the probabilistic distribution of parameters from the offline batch optimization,  $Q(\hat{\boldsymbol{\theta}})$  (see section 2.2) in HOOPE-PF. I slightly changed the parameter evolution model to include the information of  $Q(\hat{\boldsymbol{\theta}})$  into the process of the parameter perturbation after resampling. The implementation of HOOPE-PF is the following. Note that the steps from 1 to 5 are the same as the original SIRPF described in the section 2.1.

1. Forecasting the model state variables and parameters from time  $t-1$  to  $t$  using the ensemble simulation.

$$\boldsymbol{x}_i^f(t) = f(\boldsymbol{x}_i^a(t-1), \boldsymbol{\theta}_i^a(t-1), \boldsymbol{u}(t-1))$$

$$\boldsymbol{\theta}_i^f(t) = \boldsymbol{\theta}_i^a(t)$$

where superscripts  $f$  and  $a$  show forecasted and updated variables, respectively. Subscript  $i$  shows the ensemble number. No dynamics is assumed for the model parameters within the assimilation window.

2. Calculating the simulated observations for all ensembles:

$$\boldsymbol{y}_i^f(t) = h(\boldsymbol{x}_i^f(t))$$

3. Calculating the weights for all ensembles:

$$w_i = \frac{L(\boldsymbol{y}^o(t), \boldsymbol{x}_i^f(t), \boldsymbol{\theta}_i^f(t))}{\sum_{k=1}^N L(\boldsymbol{y}^o(t), \boldsymbol{x}_k^f(t), \boldsymbol{\theta}_k^f(t))}$$

where  $w_i$  is the normalized weight for the  $i$ th ensemble member, and  $N$  is the ensemble size.  $L$  is the likelihood function. In this study, the observation error follows the Gaussian distribution, so that  $L$  can be formulated as follows:

$$L = \frac{1}{\sqrt{\det(2\pi\mathbf{R})}} \exp\left(-\frac{1}{2}(\boldsymbol{y}^o(t) - \boldsymbol{y}_i^f(t))^T \mathbf{R}^{-1}(\boldsymbol{y}^o(t) - \boldsymbol{y}_i^f(t))\right)$$

where  $\mathbf{R}$  is the covariance matrix of the observation error.

4. Resampling ensemble members based on the normalized weights. The normalized weights  $w_i$  is recognized as the probability that the ensemble  $i$  is selected after

resampling. The resampled state variables and parameters are defined as  $\mathbf{x}_i^{resamp}$  and  $\boldsymbol{\theta}_i^{resamp}$ , respectively.

5. Adding the perturbation to the state variables and parameters to maintain the appropriate ensemble variances:

$$\mathbf{x}_i^a = \mathbf{x}_i^{resamp} + \boldsymbol{\varepsilon}_{i,state}$$

$$\boldsymbol{\varepsilon}_{i,state} \sim N(0, S_{state} \times Var^x)$$

$$\boldsymbol{\theta}_i^a = \boldsymbol{\theta}_i^{resamp} + \boldsymbol{\varepsilon}_{i,para}$$

$$\boldsymbol{\varepsilon}_{i,para} \sim N(0, S_{para} \times Var^\theta)$$

where  $N(\cdot)$  is the Gaussian distribution,  $Var^x$  and  $Var^\theta$  are the ensemble variances of the state variables  $\mathbf{x}_i^f(t)$  and parameters  $\boldsymbol{\theta}_i^f(t)$  in the background field, respectively.

6. Calculating the acceptance probability of  $\boldsymbol{\theta}_i^a$ ,  $\alpha(\boldsymbol{\theta}_i^{resamp}, \boldsymbol{\theta}_i^a)$  by evaluating how  $\boldsymbol{\theta}_i^a$  corresponds to the results of the offline batch optimization,  $Q(\hat{\boldsymbol{\theta}})$ :

$$\alpha(\boldsymbol{\theta}_i^{resamp}, \boldsymbol{\theta}_i^a) = \frac{Q(\boldsymbol{\theta}_i^a)}{Q(\boldsymbol{\theta}_i^{resamp})} \quad (19)$$

7. Determine if  $\boldsymbol{\theta}_i^a$  is accepted as a new parameter or not. A random number,  $b$ , is generated from the uniform distribution of  $[0,1]$ . Then,

If  $b \leq \alpha(\boldsymbol{\theta}_i^{resamp}, \boldsymbol{\theta}_i^a)$ , accept the updated parameter  $\boldsymbol{\theta}_i^a$

If  $b > \alpha(\boldsymbol{\theta}_i^{resamp}, \boldsymbol{\theta}_i^a)$ , reject the current updated parameter and go back to the step 5 only for the parameters.

By the new steps 6 and 7, I could prevent from sampling parameters which cannot support the results of the offline batch optimization. If there are no observations to be assimilated and only perturbation to parameters is performed every assimilation window for a long while, the ensemble members of the parameters converge to  $Q(\hat{\boldsymbol{\theta}})$ . I will reveal that this method substantially stabilizes PF.

### 3. Experiment design

#### 3.1. Case study I: The Lorenz 63 model with an abruptly changed parameter

I tested HOOPE-PF with the Lorenz 63 model (Lorenz 1963):

$$\frac{dx}{dt} = -10(x - y) \quad (20)$$

$$\frac{dy}{dt} = -xz + \rho(t)x - y \quad (21)$$

$$\frac{dz}{dt} = xy - bz \quad (22)$$

$\rho(t)$  and  $b$  are unknown parameters to be estimated. The true  $b$  is assumed to be  $8/3$ . Although the parameter in equation (21) is time-invariant in the original Lorenz 63 model, here I assumed that  $\rho(t)$  was a time-varying parameter:

$$\rho(t) = \begin{cases} 28 & (0 \leq t < 8000, 16000 \leq t < 24000) \\ 24 & (8000 \leq t < 16000, 24000 \leq t < 32000) \end{cases} \quad (23)$$

In this case study,  $\rho(t)$  abruptly changes every 8,000 timesteps.

The two state variables,  $y$  and  $z$ , are assumed to be observed every 20 timesteps and the observation error was set to 1.0. I set the climatological index  $\boldsymbol{\gamma} = [\overline{y^2}, \overline{z^2}]$  by averaging simulated and observed variables during 4,000 timesteps. I performed 500 ensemble runs with different (time-invariant) parameters for 4,000 timesteps to construct the surrogate model ( $g^{(s)}(\hat{\boldsymbol{\theta}})$ ). In the MCMC sampler, observations up to  $t=32000$  are used to generate the subsets of the observation timeseries (see section 2.2). I compared the performance of HOOPE-PF with that of the original PF. The other settings of the hyperparameters and the ensemble size can be found in Table 1.

### 3.2. Case study II: The Lorenz 63 model with non-periodic forcing

In this second case study, I also used the Lorenz 63 model described in equations (20-22). However, the time-varying parameter was defined as:

$$\rho(t) = \rho_o + \psi(t) \quad (24)$$

$$\psi(t) = A\left(\frac{1}{3}\sin(2\pi ft) + \frac{1}{3}\sin(\sqrt{3}ft) + \frac{1}{3}\sin(\sqrt{17}ft)\right) \quad (25)$$

where  $\rho_o = 28$ ,  $A = 5$ , and  $f = 1/20$ . This version of the Lorenz 63 model has been intensively analyzed by Daron and Stainforth (2015). The settings of observation and the climatological index are the same as the case study I. I compared the performance of HOOPE-PF with that of the original PF. The other settings of the hyperparameters and the ensemble size can be found in Table 1.

### 3.3. Case study III: Real-data experiment with the conceptual hydrological model

While the previous two case studies are the synthetic experiments, here I estimated parameters of the conceptual hydrological model, HYMOD (Moore 2007), by assimilating the real runoff observation. HYMOD has been widely used for studies on parameter optimization (e.g., Moradkhani et al. 2005a, Vrugt et al. 2013; Pathiraja et al. 2018). HYMOD consists of a nonlinear rainfall excess model connected to four linear

routing reservoirs (three quick-flow reservoirs and a slow-flow reservoir). There are 5 state variables and 5 parameters in HYMOD. Table 2 shows the description and ranges of these 5 parameters.

The study area is the Leaf River basin, Mississippi, the United States. The Leaf River basin has been used to test data assimilation and parameter optimization methods by previous works (e.g., Moradkhani et al. 2005a; Vrugt et al. 2013; Sheikholeslami and Razavi 2020). I extracted the data of precipitation, potential evapotranspiration, and runoff from the Catchment Attributes and Meteorology for Large Sample studies dataset (CAMELS; Addor et al. 2017).

The climatological index was set to the 5-year runoff ratio and the 5-year baseflow index. The runoff ratio is defined as the ratio of total runoff to total precipitation. The baseflow index is defined as the ratio of total baseflow to total runoff. The baseflow separation was performed by the one-parameter Lyne-Hollick digital filter (Lyne and Hollick 1979). Following Gnann et al. (2019), the Lyne-Hollick digital filter was applied forward, backward, and forward again using a filter parameter of 0.925.

I performed 500 ensemble runs for 5 years (from 1981-1985) to construct the surrogate model. This surrogate model directly estimates runoff ratio and baseflow index from the 5 parameters of HYMOD. In the MCMC sampler, observations from 1981-2000 were used to generate the subsets of the observation timeseries (see section 2.2). Although the HOOPE-PF was performed from 1981 to 2014, the results from 1981-2000 were not used for evaluation. The performance of HOOPE-PF was evaluated from 2001 to 2014 so that the observation data used for the offline batch optimization were not used for the evaluation of HOOPE-PF.

When the state variables are updated, I took the logarithm of them to prevent from obtaining negative values of state variables. The error variance of observed runoff was set to 10% of the observed value following Pathiraja et al. (2018). In addition, I set the minimum observation variance to 0.1 since the filter degeneracy was induced by too small observation errors. The state variables and parameters were updated by assimilating the daily runoff observation every day. I compared the performance of HOOPE-PF with the original PF. The other settings of the hyperparameters and the ensemble size can be found in Table 1.

## 4. Results

### 4.1. Case study I: The Lorenz 63 model with an abruptly changed parameter

Figure 2 shows the probabilistic distribution of parameters obtained by the offline batch optimization,  $Q(\hat{\theta})$ . Both  $\rho$  and  $b$  are distributed around the synthetic truth. Although most of observation information is not used by averaging its long-term timeseries in the offline batch optimization, the accurate posterior distribution can be obtained.

In Figure 3, the performances of HOOPE-PF and PF are evaluated by Root-Mean-Square-Error (RMSE) of  $\rho(t)$  as the function of two inflation hyperparameters (equations 10 and 12). Since it is the synthetic experiment, I can directly compare the estimated parameter with the synthetic truth of the parameter. First, HOOPE-PF outperforms PF especially when the ensemble size is small ( $N=30$ ). In HOOPE-PF, RMSE of  $\rho(t)$  is less than 1.5 in many hyperparameter settings (Figure 3d) while there are no combinations of hyperparameters which can obtain RMSE less than 1.5 in PF (Figure 3a). Second, in HOOPE-PF, the sensitivity of the hyperparameter  $S_{para}$  to RMSE of  $\rho(t)$  is much smaller than that in PF. Except for the case of the smallest  $S_{para}$ , HOOPE-PF stably provides the accurate estimation of  $\rho(t)$  especially when the ensemble size is large (Figures 3e and 3f). On the other hand, the performance of PF is substantially sensitive to  $S_{para}$  (Figures 3b and 3c). In the case of the largest  $S_{para}$ , PF collapses. This superior of HOOPE-PF to PF can also be found in RMSE of the state variables (results not shown).

Figure 4 shows the timeseries of  $\rho(t)$  in the PF and HOOPE-PF with the selected settings to demonstrate how differently these two data assimilation methods work. In the case of the smallest  $S_{para}$ , both PF and HOOPE-PF cannot accurately estimate the temporal change in the parameter since the ensemble variance is too small to detect the abrupt regime change (Figures 4a and 4e). When I increased  $S_{para}$  to 0.5, both PF and HOOPE-PF maintain the appropriate ensemble variances and successfully estimate the time-varying parameter. However, in PF, the filter becomes unstable when I further increased  $S_{para}$  and PF completely collapses in  $S_{para} = 0.9$  (Figures 4c and 4d). On the other hand, HOOPE-PF stably works in the cases of the higher  $S_{para}$  (Figures 4g and 4h). This is because the perturbed parameters are constrained by the result of the offline batch optimization in HOOPE-PF. The constraint of the offline batch optimization prevents ensemble members from going to the unrealistic space of parameters in terms of model's climate even if each ensemble member is strongly perturbed by the large  $S_{para}$ .

#### 4.2. Case study II: The Lorenz 63 model with non-periodic forcing

Figure 5 shows the probabilistic distribution of parameters obtained by the offline batch optimization,  $Q(\hat{\theta})$  in the case study II. Since true  $\rho(t)$  changes from 23 to 33 (equations (24-25)), the posterior distribution of  $\rho(t)$  obtained by the offline batch optimization captures the range of the synthetic true parameter.

Figure 6 indicates that HOOPE-PF outperforms PF in this case study as I found in the case study I. In HOOPE-PF, the change in  $\rho(t)$  can be accurately estimated when  $S_{para}$  is relatively large even if the ensemble size is small. The performance of PF is substantially sensitive to  $S_{para}$  even in the cases of the large ensemble sizes. It implies that the intensive calibration of the inflation hyperparameter is necessary if one uses no objective estimation schemes of the hyperparameters. In HOOPE-PF, this intensive hyperparameter calibration is unnecessary.

Figure 7 demonstrates that  $S_{para}$  plays the important role in controlling the ensemble variance and the skill to stably estimate the time-varying parameter in the original PF. On the other hand, the offline batch optimization largely determines the ensemble variance in HOOPE-PF and the role of  $S_{para}$  is much less important in HOOPE-PF than that in PF.

#### 4.3. Case study III: Real-data experiment with the conceptual hydrological model

Figure 8 shows the histograms of the HYMOD's 5 parameters (see Table 2) estimated by the offline batch optimization. All parameters are shown as normalized values by the prescribed maximum and minimum values (see Table2). There is no known synthetic truth in this case study since I used the real runoff observation in this experiment. The 5-year runoff ratio and baseflow index effectively constrain  $b_{exp}$  and  $k_s$ . Although the relatively large variances remain in the other three parameters, all 5 parameters sampled by MCMC are mutually correlated with each other (not shown). Therefore, the offline batch optimization substantially reduces the total volume of the parameter space which should be searched by the particle filtering.

In Figure 9, the performances of HOOPE-PF and PF are evaluated by the Kling-Gupta Efficiency (KGE, Gupta et al. 2009) as the functions of the two inflation hyperparameters. KGE changes from  $-\infty$  to 1 and the larger KGE means the better skill to reproduce

observed runoff. Figure 9 clearly reveals that HOOPE-PF outperforms PF in most cases. The effects of the two hyperparameters on the stability and accuracy of simulations in this case study are different from those in the previous case studies. The performance of PF is not degraded when  $S_{para}$  is set to the large values. This is mainly because the model parameters are bounded in the reasonable prescribed ranges shown in Table 2, which prevents the filter from collapsing when the ensemble variance of parameters is strongly inflated. In this case study, ensemble members are already constrained by the prescribed ranges shown in Table 2, which stabilizes the original PF. The offline batch optimization further constrains ensemble members to the regions in which the observed runoff ratio and baseflow index can be reasonably reproduced. This additional constraint by the offline batch optimization significantly improves KGE.

Figure 10 demonstrates the difference between HOOPE-PF and PF by showing the timeseries of runoff and  $k_q$  (see Table 2). Although PF accurately estimates flood peaks in many cases except for the flood peak in April 2002, PF overestimates baseflow (Figure 10a). This is probably because the model parameters overfit the flood events and fail to adapt the rapid phase changes from high flow to baseflow due to the small ensemble variance in the observation space. On the other hand, HOOPE-PF successfully simulates both high flow and baseflow (Figure 10b). The temporal change of  $k_q$  in HOOPE-PF is stabler than that in the original PF (Figures 10c and 10d). In HOOPE-PF,  $k_q$  rapidly increases only in the flood periods. It is generally difficult for hydrological models with a single set of parameters to accurately simulate runoff in both wet and dry periods (e.g., Deb and Kiem 2020). The application of HOOPE-PF to HYMOD overcomes this limitation by allowing model parameters to abruptly change based on the observed runoff.

## 5. Conclusions and discussion

Here I present the new efficient and practical method to estimate model parameters allowing them to temporally change by combining the offline batch optimization and the online data assimilation. In the newly proposed method, HOOPE-PF, I constrain the estimated model parameters in the sequential data assimilation to the result of the offline batch optimization in which the posterior distribution of model parameters is obtained by comparing the simulated and observed climatology. The HOOPE-PF outperforms the original sampling-importance-resampling particle filter in the synthetic experiment with the Lorenz 63 model and the real-data experiment of the rainfall-runoff analysis. The advantage of HOOPE-PF is that the performance of the online data assimilation is not



greatly affected by the “inflation” hyperparameter for model parameters while this hyperparameter has been sensitive to the performance in many previous methods and how to objectively determine it has been intensively discussed in the previous works (e.g., Moradkhani et al. 2005a, 2005b; Moradkhani et al. 2012; Ruiz et al. 2013; Kotsuki et al. 2019).

The proposed HOOPE-PF can be the practical approach to detect and quantify the unmodelled processes such as land use change (e.g., Pathiraja et al. 2018) from the long-term observation. In addition, the modeling with time-varying parameters by HOOPE-PF realized the stochastic process models whose potential was intensively discussed by Reichert et al. (2021). Reichert et al. (2021) clearly shows that the stochastic process models with time-varying parameters have the advantage to identify the intrinsic model uncertainty and improve the model processes.

There are three limitations in HOOPE-PF. First, since HOOPE-PF requires the long-term observation before beginning the real-time online estimation, it cannot be applied to some types of the real-time estimation problem in which there is no observation at the initial time and the estimation of state variables and parameters needs to be gradually improved whenever new observations are obtained. This situation is often assumed in the previous works about data assimilation on groundwater modelling (e.g., Hendrick-Franssen et al. 2008; Ramgraber et al. 2019) although the long-term observation timeseries can be obtained in many geoscientific applications such as numerical weather prediction and rainfall-runoff analysis.

Second, there is no generally applicable way to construct the appropriate “climatological index” for the offline batch optimization (equation (15)). Equation (15) needs to be the summary of the climatology of the important process for a user’s purpose. It should be independent to the initial condition. The design of equation (15) apparently depends on the problems. The design of the appropriate climatological index for the offline batch optimization is generally challenging (e.g., Springer et al. 2021). It is promising that the climatological index based only on the widely used hydrological indices, runoff ratio and baseflow index, appropriately works in the application of HOOPE-PF to the conceptual hydrological model. It implies that no complicated methods are needed to construct equation (15).

Third, the current HOOPE-PF cannot be directly applied to the high-dimensional problems because the number of ensemble members required increases exponentially with the size of problems (e.g., Snyder et al. 2008). The recent progress on the application of PF to the high-dimensional problem (i.e. numerical weather prediction) (e.g., Poterjoy et al. 2019; Kawabata and Ueno 2020) needs to be included to directly apply HOOPE-PF to optimize the parameters of the high-dimensional models. In addition, the fundamental idea of HOOPE-PF can be transferred to EnKF which has been successfully applied to the high-dimensional problems. The future work will be to develop the version of ensemble Kalman filter (HOOPE-EnKF) based on the similar strategy which I showed in this paper.

### Acknowledgements

The CAMELS dataset can be downloaded at <https://ral.ucar.edu/solutions/products/camels>. I thank Kel Markert for providing the useful Python source code of the HYMOD model which was used in this paper and can be downloaded at <https://github.com/KMarkert/hymod>. The study was supported by the JST FOREST program (grant no. JPMJFR205Q), the KAKENHI grant (grant no. 21H01430), and the Foundation of River & basin Integrated CommunicationS (FRICS).

### References

- Abbaszadeh, P., Moradkhani, H., & Yan, H. (2018). Enhancing hydrologic data assimilation by evolutionary Particle Filter and Markov Chain Monte Carlo. *Advances in Water Resources*, 111, 192–204. <https://doi.org/10.1016/j.advwatres.2017.11.011>
- Addor, N., Newman, A., J., Muzukami, N., Clark, M., P. (2017). The CAMELS data set: catchment attributes and meteorology for large-sample studies. *Hydrology and Earth System Sciences*, 21, 5293-5313. <https://doi.org/10.5194/hess-21-5293-2017>
- Ait-El-Fquih, B., & Hoteit, I. (2017). An Efficient State-Parameter Filtering Scheme Combining Ensemble Kalman and Particle Filters. *Monthly Weather Review*, MWR-D-16-0485.1. <https://doi.org/10.1175/MWR-D-16-0485.1>
- Anderson, J. L. (2007). Exploring the need for localization in ensemble data assimilation using a hierarchical ensemble filter. *Physica D: Nonlinear Phenomena*, 230(1–2), 99–111. <https://doi.org/10.1016/j.physd.2006.02.011>
- Cleary, E., Garbuno-Inigo, A., Lan, S., Schneider, T., & Stuart, A. M. (2021). Calibrate, emulate, sample. *Journal of Computational Physics*, 424, 109716. <https://doi.org/10.1016/j.jcp.2020.109716>

- Constantine, P. G., Dow, E., & Wang, Q. (2014). Active subspace methods in theory and practice: Applications to kriging surfaces. *SIAM Journal of Scientific Computing*, 36(4), A1500–A1524. <https://doi.org/10.1137/130916138>
- Daron, J., D., & Stainforth, D., A (2015). On quantifying the climate of the nonautonomous Lorenz-63 model. *Chaos*, 25, 043103, <https://doi.org/10.1063/1.4916789>
- Deb, P. & Kiem, A., S. (2020). Evaluation of rainfall–runoff model performance under non-stationary hydroclimatic conditions, *Hydrological Sciences Journal*, 65, 1667–1684, <https://doi.org/10.1080/02626667.2020.1754420>
- Di Baldassarre, G., Viglione, A., Carr, G., Kuil, L., Salinas, J. L., & Blöschl, G. (2013). Socio-hydrology: Conceptualising human-flood interactions. *Hydrology and Earth System Sciences*, 17(8), 3295–3303. <https://doi.org/10.5194/hess-17-3295-2013>
- Dunbar, O. R. A., Garbuno-Inigo, A., Schneider, T., & Stuart, A. M. (2021). Calibration and uncertainty quantification of convective parameters in an idealized GCM. *Journal of Advances in Modeling Earth Systems*, 13, e2020MS002454. <https://doi.org/10.1029/2020MS002454>
- Gnann, S. J., Woods, R. A., & Howden, N. J. K. (2019). Is There a Baseflow Budyko Curve? *Water Resources Research*, 2838–2855. <https://doi.org/10.1029/2018WR024464>
- Gupta, H. V., Kling, H., Yilmaz, K. K., & Martinez, G. F. (2009). Decomposition of the mean squared error and NSE performance criteria: Implications for improving hydrological modelling. *Journal of Hydrology*, 377(1–2), 80–91. <https://doi.org/10.1016/j.jhydrol.2009.08.003>
- Hastings, W. K. (1970). Monte Carlo sampling methods using Markov chains and their applications. *Biometrika*, 57(1), 97–109. <https://doi.org/10.1093/biomet/57.1.97>
- Hendricks Franssen, H. J., & Kinzelbach, W. (2008). Real-time groundwater flow modeling with the Ensemble Kalman Filter: Joint estimation of states and parameters and the filter inbreeding problem. *Water Resources Research*, 44(9), 1–21. <https://doi.org/10.1029/2007WR006505>
- Hunt, B. R., Kostelich, E. J., & Szunyogh, I. (2007). Efficient data assimilation for spatiotemporal chaos: A local ensemble transform Kalman filter. *Physica D: Nonlinear Phenomena*, 230(1–2), 112–126. <https://doi.org/10.1016/j.physd.2006.11.008>
- Kawabata, T., & Ueno, G. (2020). Non-Gaussian probability densities of convection initiation and development investigated using a particle filter with a storm-scale

- numerical weather prediction model. *Monthly Weather Review*, 148(1), 3–20. <https://doi.org/10.1175/MWR-D-18-0367.1>
- Kotsuki, S., Terasaki, K., Yashiro, H., Tomita, H., Satoh, M., & Miyoshi, T. (2018). Online model parameter estimation with ensemble data assimilation in the real global atmosphere: A case with the Nonhydrostatic Icosahedral Atmospheric Model (NICAM) and the Global Satellite Mapping of Precipitation data. *Journal of Geophysical Research: Atmospheres*, 123, 7375–7392. <https://doi.org/10.1029/2017JD028092>
- Laloy, E., & Vrugt, J. A. (2012). High-dimensional posterior exploration of hydrologic models using multiple-try DREAM (ZS) and high-performance computing. *Water Resources Research*, 48(1), 1–18. <https://doi.org/10.1029/2011WR010608>
- Leisenring, M. & Moradkhani, H. (2012). Analyzing the uncertainty of suspended sediment load prediction using sequential data assimilation. *Journal of Hydrology*, 468-469, 268-282. <https://doi.org/10.1016/j.jhydrol.2012.08.049>
- Liu, J. & West, M. (2001) Combined parameter and state estimation in simulation-based filtering. In *Sequential Monte Carlo Methods in Practice* (eds A. Doucet, N. de Freitas and N. J. Gordon), pp. 197–223. New York: Springer.
- Lorenz, E. N. (1963). Deterministic Nonperiodic Flow. In *Journal of the Atmospheric Sciences* (Vol. 20, Issue 2, pp. 130–141). [https://doi.org/10.1175/1520-0469\(1963\)020<0130:DNF>2.0.CO;2](https://doi.org/10.1175/1520-0469(1963)020<0130:DNF>2.0.CO;2)
- Lunderman, S., Morzfeld, M., & Posselt, D., J. (2021) Using global Bayesian optimization in ensemble data assimilation: parameter estimation, tuning localization and inflation, or all of the above, *Tellus A: Dynamic Meteorology and Oceanography*, 73, 1-16, <https://doi.org/10.1080/16000870.2021.1924952>
- Lyne, V., and M. Hollick (1979), *Stochastic Time-Variable Rainfall-Runoff Modelling*, pp. 89–93, Inst. of Eng. Aust. Natl. Conf., Perth, Australia.
- Moore, R., J. (2007). The PDM rainfall-runoff model. *Hydrology and Earth System Sciences*, 11, 483-499, <https://doi.org/10.5194/hess-11-483-2007>
- Moradkhani, H., Hsu, K. L., Gupta, H., & Sorooshian, S. (2005a). Uncertainty assessment of hydrologic model states and parameters: Sequential data assimilation using the particle filter. *Water Resources Research*, 41(5), 1–17. <https://doi.org/10.1029/2004WR003604>
- Moradkhani, H., Sorooshian, S., Gupta, H., V., & Houser, P., R. (2005b). Dual state–parameter estimation of hydrological models using ensemble Kalman filter, *Advances in Water Resources*, 28, 135-147, <https://doi.org/10.1016/j.advwatres.2004.09.002>

- Moradkhani, H., DeChant, C. M., & Sorooshian, S. (2012), Evolution of ensemble data assimilation for uncertainty quantification using the particle filter-Markov chain Monte Carlo method, *Water Resources Research*, 48, W12520, <https://doi.org/10.1029/2012WR012144>.
- Pathiraja, S., Marshall, L., Sharma, A., & Moradkhani, H. (2016), Hydrologic modeling in dynamic catchments: A data assimilation approach, *Water Resources Research*, 52, 3350– 3372, <https://doi.org/10.1002/2015WR017192>
- Pathiraja, S., Anghileri, D., Burlando, P., Sharma, A., Marshall, L., & Moradkhani, H. (2018). Time-varying parameter models for catchments with land use change: The importance of model structure. *Hydrology and Earth System Sciences*, 22(5), 2903–2919. <https://doi.org/10.5194/hess-22-2903-2018>
- Ramgraber, M., Albert, C., & Schirmer, M. (2019). Data Assimilation and Online Parameter Optimization in Groundwater Modeling Using Nested Particle Filters. *Water Resources Research*, 55(11), 9724–9747. <https://doi.org/10.1029/2018WR024408>
- Rasmussen, C. E., & Williams, C. K. I. (2006). *Gaussian processes for machine learning*. Cambridge, MA: the MIT Press. ISBN 026218253X
- Ruiz, J., J., Pulido, M, & Miyoshi, T. (2013), Estimating Model Parameters with Ensemble-Based Data Assimilation: Parameter Covariance Treatment, *Journal of the Meteorological Society of Japan*, 91, 453-469, <https://doi.org/10.2151/jmsj.2013-403>
- Sawada, Y., & Hanazaki, R. (2020). Socio-hydrological data assimilation: Analyzing human-flood interactions by model-data integration. *Hydrology and Earth System Sciences*, 24(10). <https://doi.org/10.5194/hess-24-4777-2020>
- Sawada, Y. (2020). Machine Learning Accelerates Parameter Optimization and Uncertainty Assessment of a Land Surface Model. *Journal of Geophysical Research: Atmospheres*, 125(20). <https://doi.org/10.1029/2020JD032688>
- Sheikholeslami, R., & Razavi, S. (2020). A Fresh Look at Variography: Measuring Dependence and Possible Sensitivities Across Geophysical Systems From Any Given Data. *Geophysical Research Letters*, 47(20), 1–11. <https://doi.org/10.1029/2020GL089829>
- Snyder, C., Bengtsson, T., Bickel, P., & Anderson, J. (2008). Obstacles to High-Dimensional Particle Filtering. *Monthly Weather Review*, 136(12), 4629–4640. <https://doi.org/10.1175/2008MWR2529.1>
- Springer, S., Haario, H., Susiluoto, J., Bibov, A., Davis, A., & Marzouk, Y. (2021). Efficient Bayesian inference for large chaotic dynamical systems. *Geoscientific Model Development*, 14, 4319-4333. <https://doi.org/10.5194/gmd-14-4319-2021>

- Teixeira Parente, M., Bittner, D., Mattis, S. A., Chiogna, G., & Wohlmuth, B. (2019). Bayesian calibration and sensitivity analysis for a karst aquifer model using active subspaces. *Water Resources Research*, 55, 7086–7107. <https://doi.org/10.1029/2019WR024739>
- Poterjoy, J., Wicker, L., & Buehner, M. (2019). Progress toward the application of a localized particle filter for numerical weather prediction. *Monthly Weather Review*, 147(4), 1107–1126. <https://doi.org/10.1175/MWR-D-17-0344.1>
- Reichert, P., Ammann, L., & Fenicia, F. (2021). Potential and Challenges of Investigating Intrinsic Uncertainty of Hydrological Models With Stochastic, Time-Dependent Parameters. *Water Resources Research*, 57(3), 1–28. <https://doi.org/10.1029/2020WR028400>
- Tomizawa, F., & Sawada, Y. (2021). Combining ensemble Kalman filter and reservoir computing to predict spatiotemporal chaotic systems from imperfect observations and models. *Geoscientific Model Development*, 14, 5623–5635, <https://doi.org/10.5194/gmd-14-5623-2021>
- Vrugt, J. A., ter Braak, C. J. F., Diks, C. G. H., & Schoups, G. (2013). Hydrologic data assimilation using particle Markov chain Monte Carlo simulation: Theory, concepts and applications. *Advances in Water Resources*, 51, 457–478. <https://doi.org/10.1016/j.advwatres.2012.04.002>
- Whitaker, J. S., & Hamill, T. M. (2012). Evaluating methods to account for system errors in ensemble data assimilation. *Monthly Weather Review*, 140, 3078 - 3089. <https://doi.org/10.1175/MWR-D-11-00276.1>
- Yan, H., & Moradkhani, H. (2016). Combined assimilation of streamflow and satellite soil moisture with the particle filter and geostatistical modeling. *Advances in Water Resources*, 94, 364–378. <https://doi.org/10.1016/j.advwatres.2016.06.002>
- Zhang, J., Zheng, Q., Chen, D., Wu, L., & Zeng, L. (2020). Surrogate-Based Bayesian Inverse Modeling of the Hydrological System: An Adaptive Approach Considering Surrogate Approximation Error. *Water Resources Research*, 56(1), 1–25. <https://doi.org/10.1029/2019WR025721>

**Table 1.** Summary and detailed settings of the case studies in this paper

Name	Model	ensemble size	$S_{state}$	$S_{para}$
Case Study I	Lorenz63 with a time-varying parameter (equation (23))	[30,100,250]	[0.15,0.20,0.25,0.30,0.35]	[0.01,0.03,0.05,0.07,0.09]
Case Study II	Lorenz63 with a time-varying parameter (equations (24-25))	[30,100,250]	[0.15,0.20,0.25,0.30,0.35]	[0.01,0.03,0.05,0.07,0.09]
Case Study III	HYMOD	[30,100,250]	[0.001,0.003,0.005,0.007,0.009]	[0.01,0.03,0.05,0.07,0.09]

**Table 2.** Parameters of the HYMOD model.

Symbols	Description	Units	Range
$C_{max}$	Maximum soil storage depth	[mm]	[10, 8000]
$b_{exp}$	Pareto-distributed soil storage shape parameter	[-]	[0.1, 2.0]
$\alpha$	Excess runoff splitting parameter	[-]	[0.01, 0.99]
$k_s$	Slow flow routing coefficient	[-]	[0.001, 0.200]
$k_q$	Quick flow routing coefficient	[-]	[0.200, 0.990]



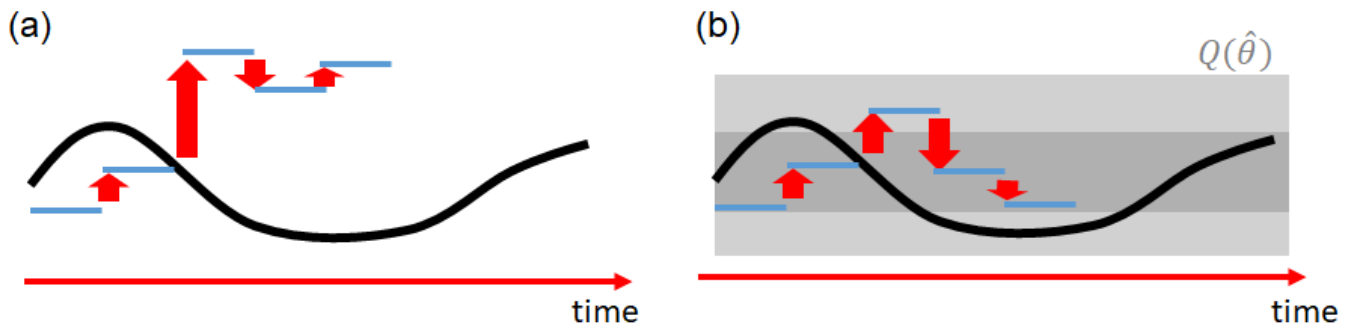


**Figure 1.** Schematics of the (a) original PF and (b) HOOPE-PF. Black lines are timeseries of the true model parameter. Blue lines are the estimation of the online data assimilation algorithm and red arrows show the adjustments by the data assimilation steps. The grey area in (b) shows the posterior distribution of the model parameter calculated by the offline batch optimization. See also section 2.3.

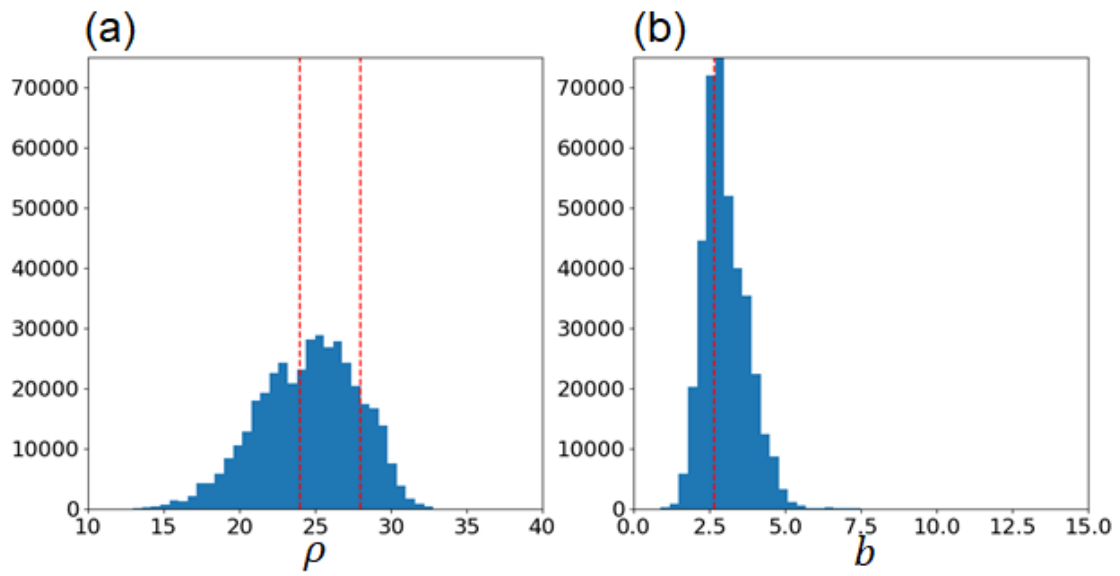


**Figure 2.** Histograms of (a)  $\rho(t)$  and (b)  $b$  of the Lorenz 63 model estimated by the MCMC sampler in the case study I (see sections 3.1. and 4.1). Red dashed lines are the synthetic truth of the model parameters.

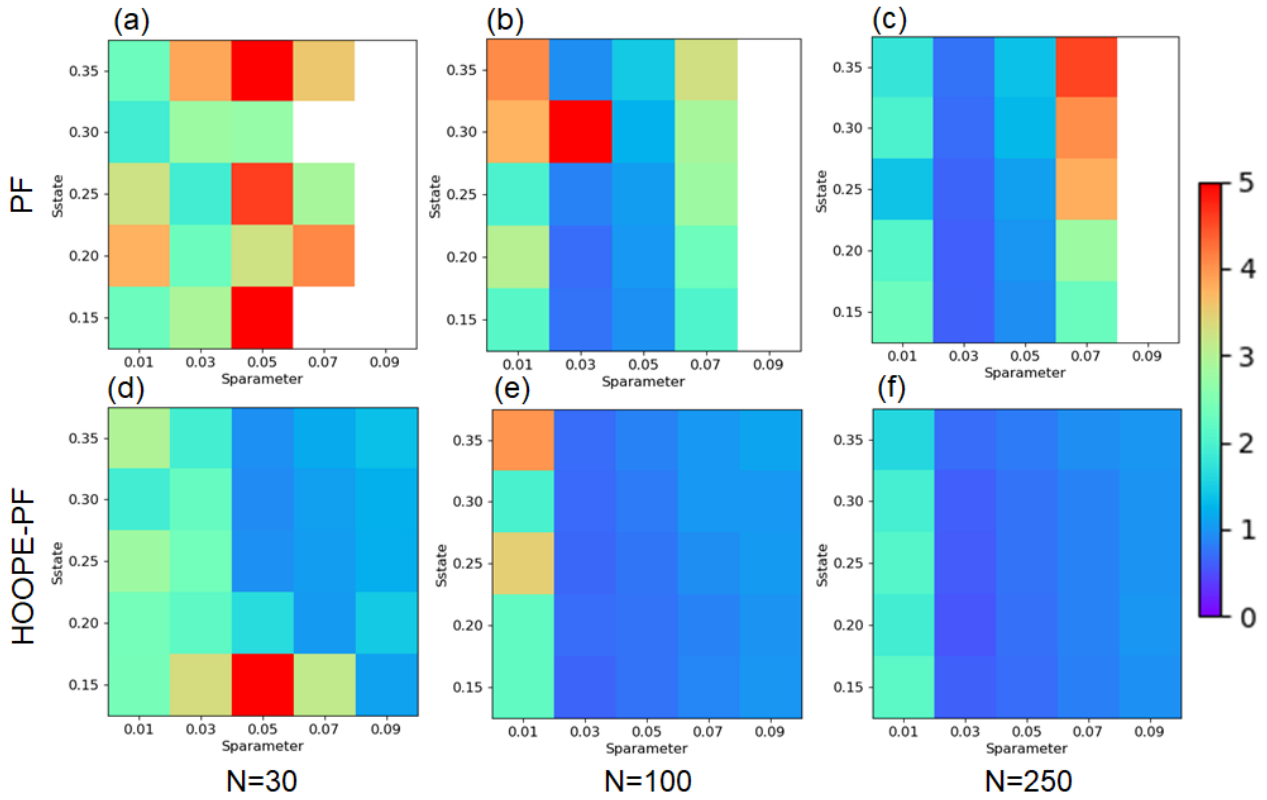


**Figure 3.** (a-c) RMSE between the synthetic true  $\rho(t)$  and the ensemble median  $\rho(t)$  estimated by the original PF with the ensemble size of (a) 30, (b) 100, and (c) 250 in the case study I (see sections 3.1 and 4.1). Horizontal and vertical axes show  $S_{para}$  and  $S_{state}$ , respectively. (d-f) same as (a-c) but for HOOPE-PF.

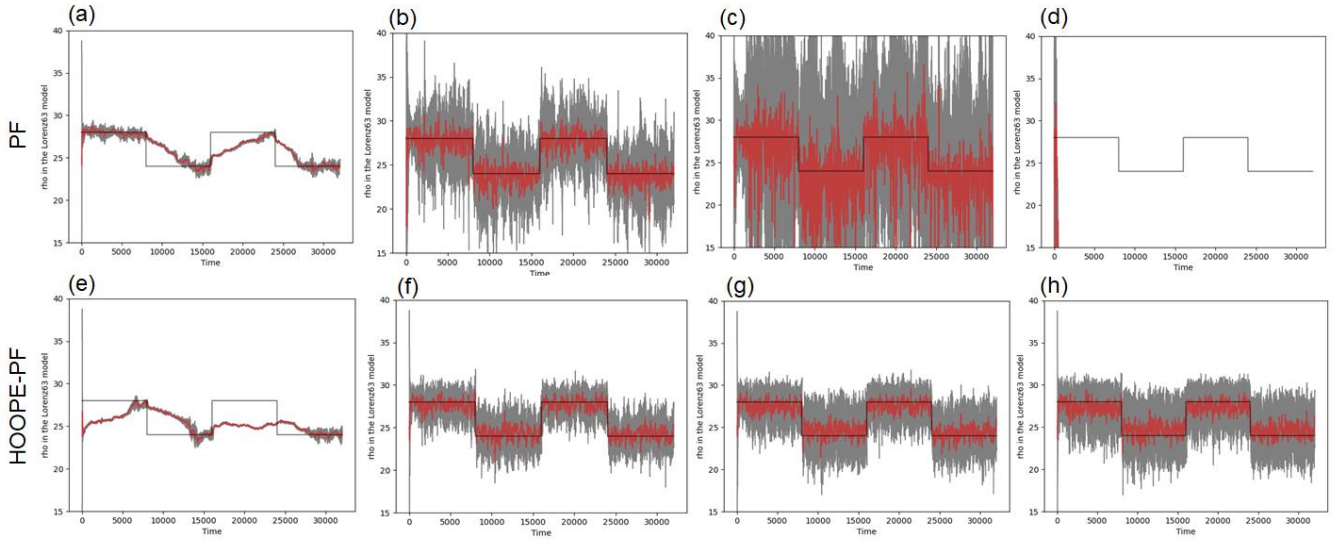


**Figure 4.** (a-d) Timeseries of  $\rho(t)$  by the original PF in the case study I (see sections 3.1 and 4.1). Black and red lines show the synthetic truth and the median of the estimated parameter by the online data assimilation, respectively. Grey areas show the 5-95 percentile range. The ensemble size is set to 250.  $S_{state}$  is set to 0.25.  $S_{para}$  is set to (a) 0.1, (b) 0.5, (c) 0.7, and (d) 0.9. (e-h) same as (a-d) but for HOOPE-PF.

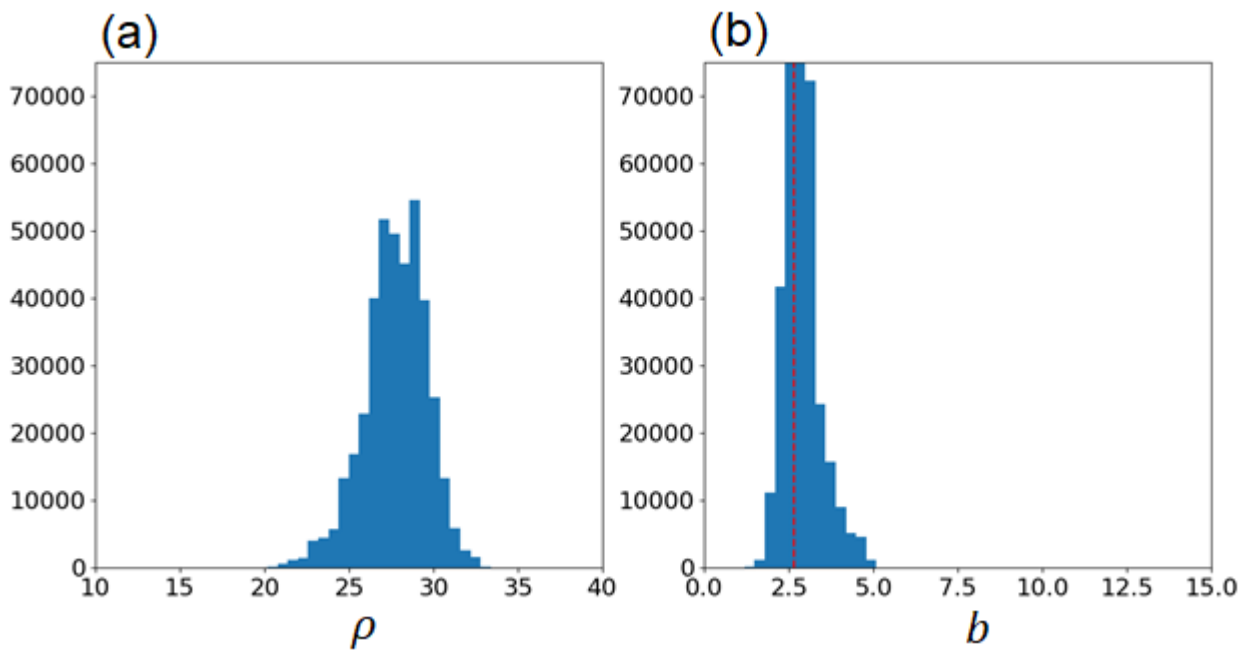


**Figure 5.** Histograms of (a)  $\rho(t)$  and (b)  $b$  of the Lorenz 63 model estimated by the MCMC sampler in the case study II (see sections 3.2. and 4.2). Red dashed line is the synthetic truth of the model parameters.

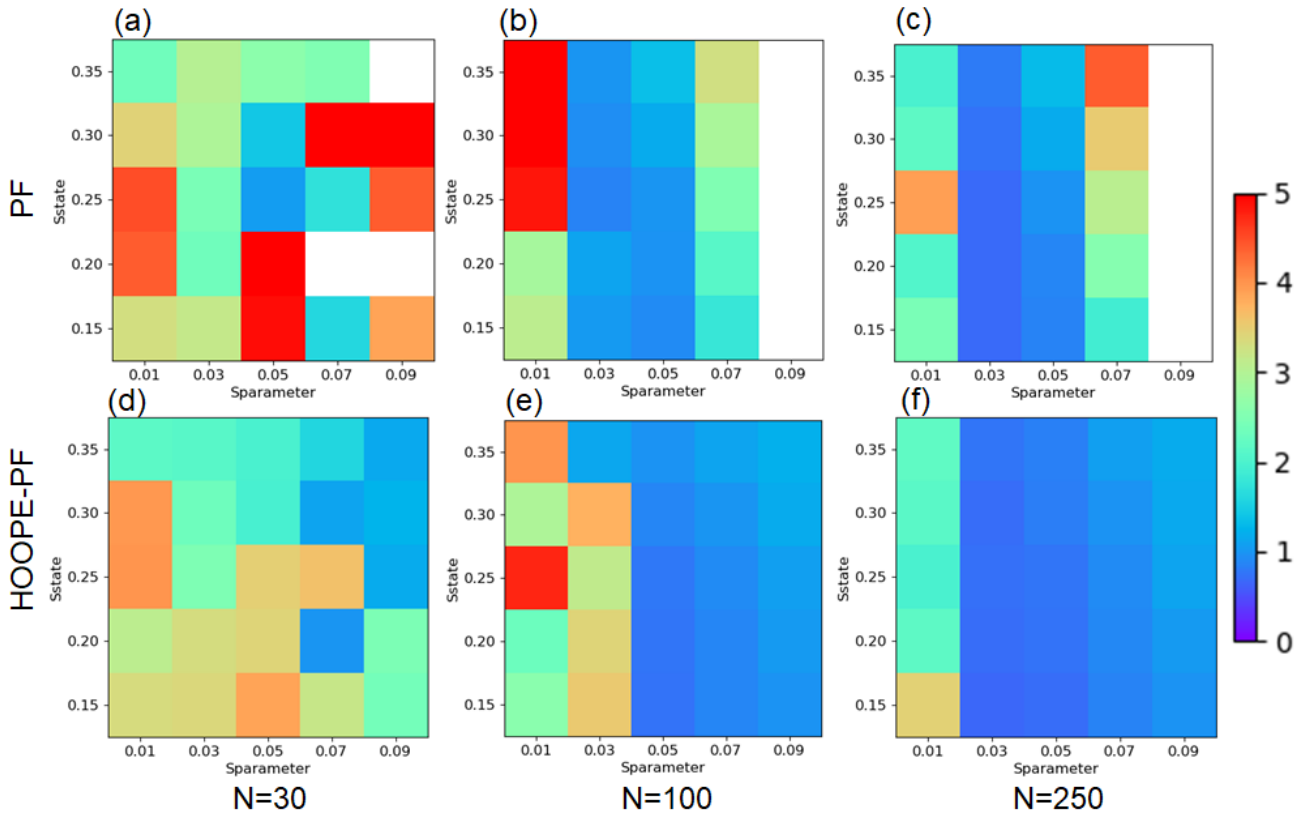


**Figure 6.** (a-c) RMSE between the synthetic true  $\rho(t)$  and the ensemble median  $\rho(t)$  estimated by the original PF with the ensemble size of (a) 30, (b) 100, and (c) 250 in the case study II (see sections 3.2 and 4.2). Horizontal and vertical axes show  $S_{para}$  and  $S_{state}$ , respectively. (d-f) same as (a-c) but for HOOPE-PF.

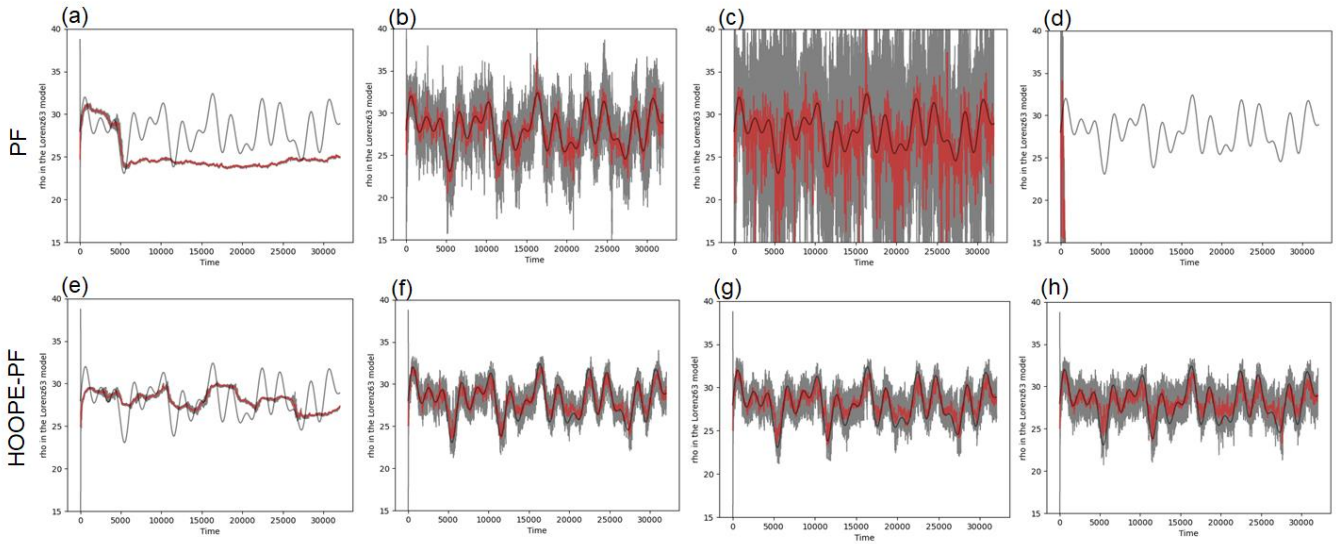


**Figure 7.** (a-d) Timeseries of  $\rho(t)$  by the original PF in the case study II (see sections 3.2 and 4.2). Black and red lines show the synthetic truth and the median of the estimated parameter by the online data assimilation, respectively. Grey areas show the 5-95 percentile range. The ensemble size is set to 250.  $S_{state}$  is set to 0.25.  $S_{para}$  is set to (a) 0.1, (b) 0.5, (c) 0.7, and (d) 0.9. (e-h) same as (a-d) but for HOOPE-PF.

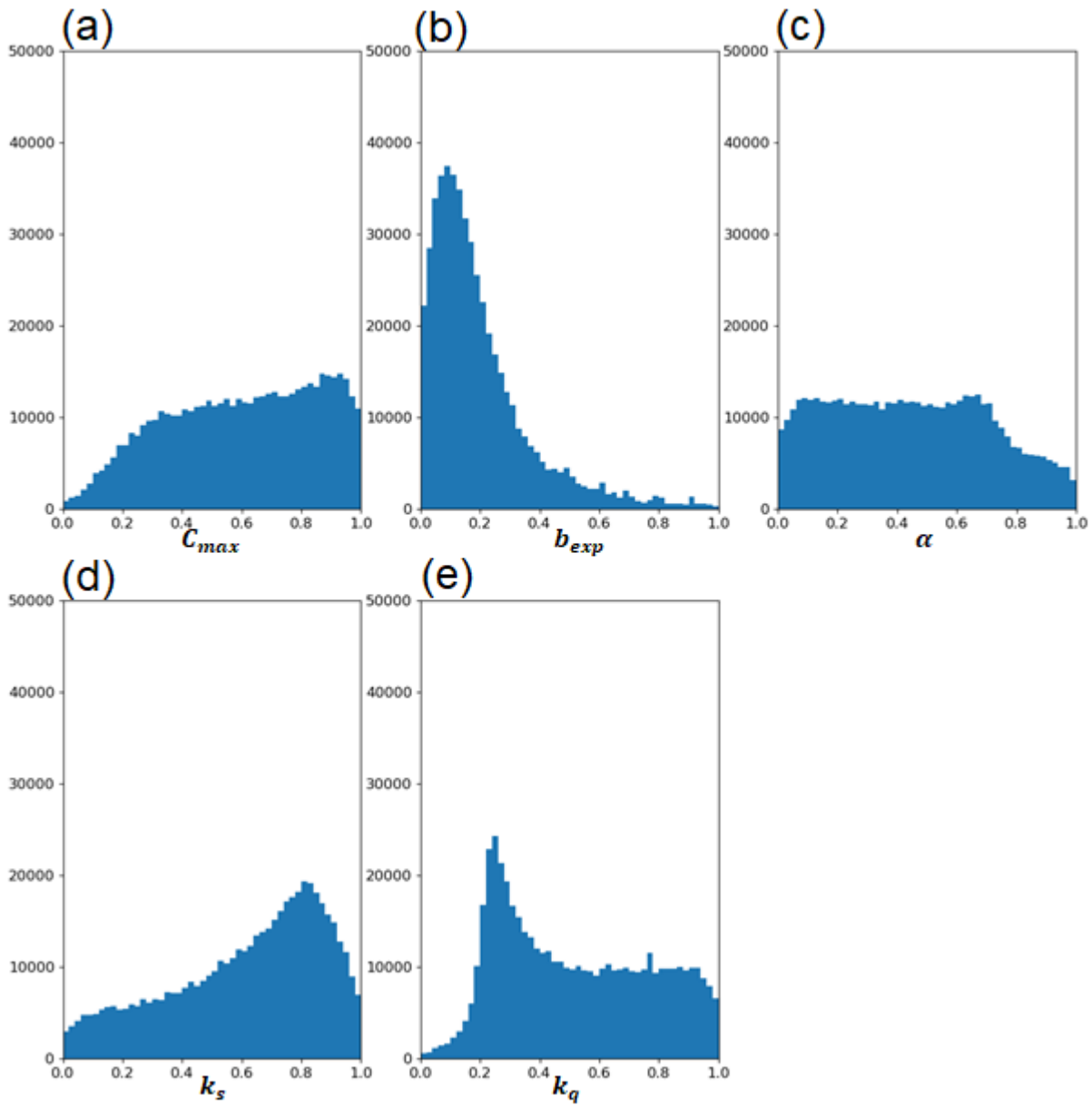


**Figure 8.** Histograms of (a)  $C_{max}$ , (b)  $b_{exp}$ , (c)  $\alpha$ , (d)  $k_s$ , and (e)  $k_q$  of the HYMOD model estimated by the MCMC sampler in the case study III (see sections 3.3. and 4.3).



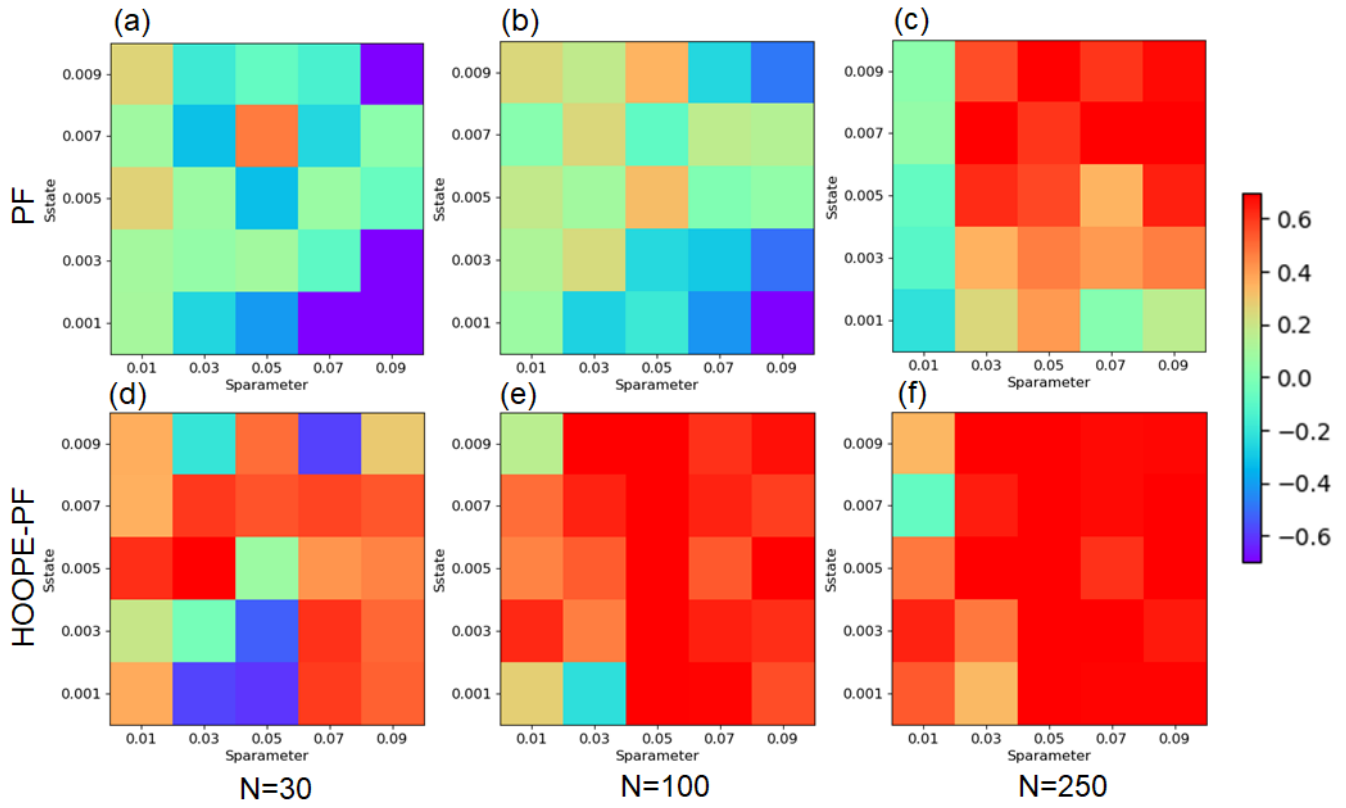


**Figure 9.** (a-c) KGE between the observed and the estimated runoff in the Leaf River by the original PF with the ensemble size of (a) 30, (b) 100, and (c) 250 in the case study III (see sections 3.3 and 4.3). The ensemble median is used as the simulated runoff. Horizontal and vertical axes show  $S_{para}$  and  $S_{state}$ , respectively. (d-f) same as (a-c) but for HOOPE-PF.

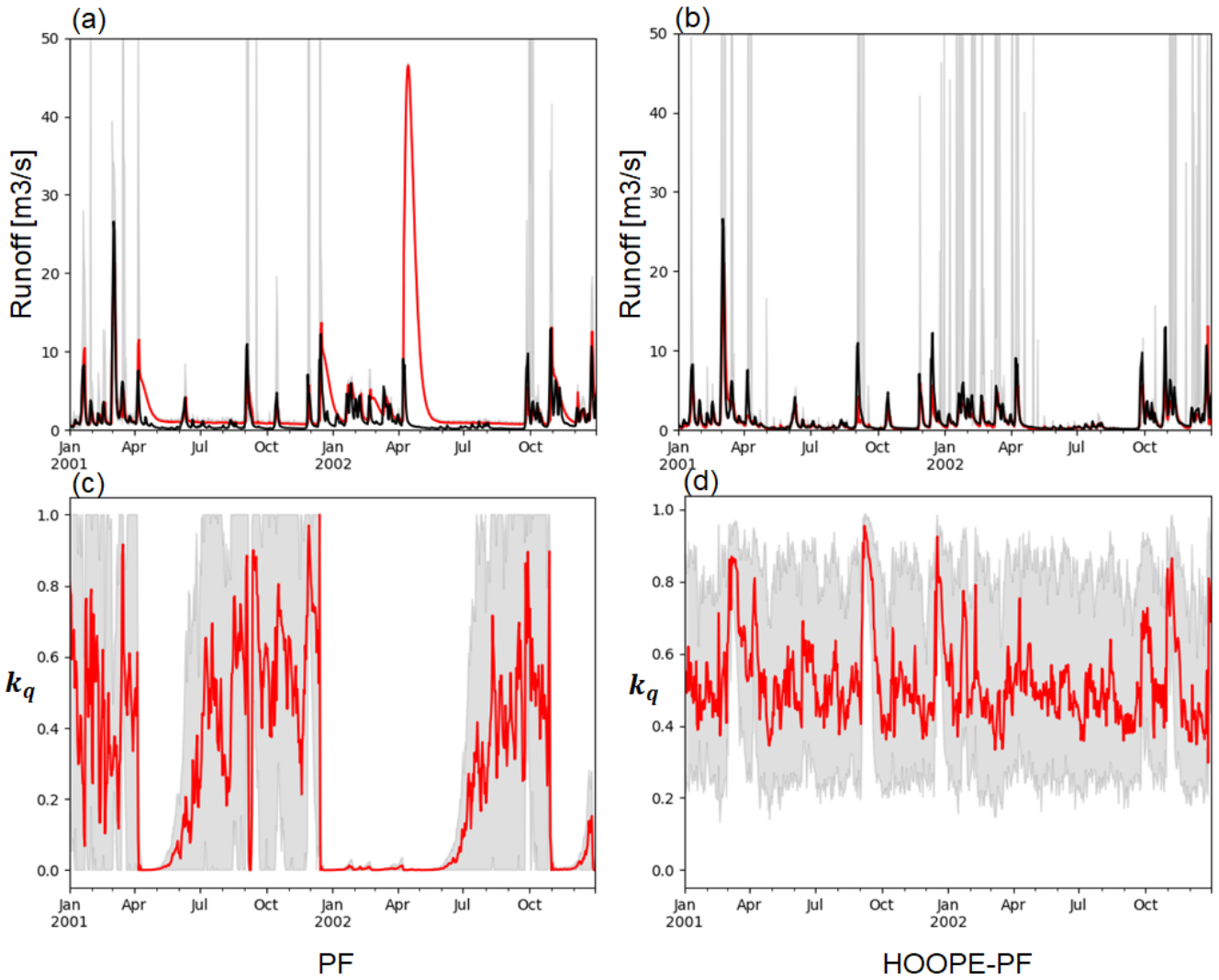


**Figure 10.** (a-b) Timeseries of daily discharge in the Leaf River basin. Black line shows the observed river discharge. Red lines and grey areas show median and the 10-90 percentile range of simulated river discharge by (a) PF and (b) HOOPE-PF. (c-d) Timeseries of the normalized quick flow routing coefficient (see Table 2) in the Leaf River basin. Red lines and grey areas show median and the 10-90 percentile range of the simulated normalized quick flow routing coefficient by (c) PF and (d) HOOPE-PF.